American Mineralogist, Volume 92, pages 1899–1911, 2007

Thermal diffusivity of aluminous spinels and magnetite at elevated temperature with implications for heat transport in Earth's transition zone

ANNE M. HOFMEISTER*

Department of Earth and Planetary Sciences, Washington University, 1 Brookings Drive, St. Louis, Missouri 63130-4899, U.S.A.

ABSTRACT

The phonon component of thermal diffusivity (D) from 12 single crystals in the spinel family was measured at temperatures (T) of up to ~2000 K, using laser-flash analysis. Synthetic disordered spinel, 4 gemstones near $MgAl_2O_4$, nearly $ZnAl_2O_4$, 4 "hercynites" [$(Mg,Fe^{2+})(Al,Fe^{3+})_2O_4$], and 2 magnetites (nearly Fe_3O_4) were characterized using optical spectroscopy and electron microprobe analysis. The magnetic transition in Fe_3O_4 is manifest as a lambda curve in $1/D$, but otherwise, D decreases with increasing T and approaches a constant (D_{sat}) at high T. Part of the decrease in D as T increases results from disordering above ~700 K: these two effects were distinguished by making multiple heating runs. At 298 K, D decreases strongly as either cation substitution or Mg-Al disorder increases, whereas D_{sat} is moderately perturbed by substitutions. For both ordered and (equilibrium) disordered spinels and hercynites, the temperature dependence of $1/D$ is best described by low-order polynomial fits. For spinel, combining our data with previous cryogenic studies of thermal conductivity (k) constrains the T dependence of D and k from ~0 K to melting.

The response of D to disorder, impurity content, and cation mass for the aluminates is used to constrain $D(T)$ for γ-Mg_2SiO_4 and ringwoodite. Pressure derivatives are provided by relationships such as $\partial\ln(k_{lat})/\partial P = \partial\ln(K_T)/\partial P$. Our results show that the phonon contribution to heat transport in Earth's transition zone is high, particularly for large proportions of ringwoodite.

Keywords: Laser-flash method, high temperature, thermal diffusivity, IR spectroscopy, spinel-family minerals, high pressure, aluminates

INTRODUCTION

Minerals crystallizing in the spinel structure occur as widespread accessory phases in part due to the ability of this structure to accommodate diverse cations. Within the transition zone of Earth's mantle, olivine converts to spinel and spinel-like structures. Therefore, knowing the physical properties for the spinel group pertains to both geology and geophysics. In particular, heat transfer properties of minerals are poorly constrained, yet bear on environments where spinel-family minerals occur, such as subducting slabs or metamorphic terrains.

For spinels, thermal diffusivity (D) or thermal conductivity

$$k = \rho C_P D \quad (1)$$

have only been studied by contact methods (Slack 1962; Xu et al. 2004), which underestimate k or D near 298 K due to losses at interfaces but overestimate results above ~700 K due to unwanted radiative (photon) transfer (e.g., Hofmeister 2006, 2007; Pertermann and Hofmeister 2006; Hofmeister et al. 2007). The present report uses the contact-free laser-flash technique (e.g., Parker et al. 1961; Mehling et al. 1998) which removes spurious *photon* transfer and accurately (~2% uncertainty) provides the component of heat transfer originating through *phonon* scattering (lattice conductivity, k_{lat}). To ascertain the effect of crystal chemistry for spinel-family minerals, we examined five samples that differ slightly from $MgAl_2O_4$ (caused either by cation substitution or disorder), nearly end-member gahnite ($ZnAl_2O_4$), four hercynites [essentially $(Mg,Fe^{2+})(Al,Fe^{3+})_2O_4$], and two near end-member magnetites (Fe_3O_4). Specimens were characterized by electron microprobe analysis and optical spectroscopy. Published crystallographic data on Mg-Al disordering in spinel were used to interpret our results. Comparison with the damped harmonic oscillator (DHO)-phonon gas model (e.g., Hofmeister 1999, 2007) is made to better understand microscopic behavior during heat transport. Values for ringwoodite are inferred, and implications for Earth's transition zone are discussed.

EXPERIMENTAL METHODS

Sample preparation

Samples were cut, ground, and polished into slabs of 6–11 mm diameter with thicknesses of 0.3–3.5 mm. After spectroscopic and electron microprobe measurements, samples were sandblasted with alumina grit of 50–150 μm to roughen the surface. Finally, a graphite coating was applied as 3–5 thin layers on each surface. Total coating thicknesses of ~1 μm negligibly affect measurements of D from our roughly millimeter-sized samples.

Electron microprobe analyses

All samples were characterized chemically by wavelength dispersive analysis (WDS) using standard procedures on the JEOL-733 electron microprobe at Washington University. Synthetic and natural mineral and oxide standards (e.g., ilmenite) were used for calibration.

* E-mail: hofmeist@levee.wustl.edu

0003-004X/07/1112–1899$05.00/DOI: 10.2138/am.2007.2589

Near-IR to visible spectroscopy

We used an evacuated Bomem DA3.02 Fourier transform interferometer with a SiC source, a HgCdTe detector, and a KBr beamsplitter. Instrumental accuracy is 0.01 cm^{-1}. About 2000 scans were collected at room temperature from ~1200–4000 cm^{-1} at a resolution of 4 cm^{-1}. Using an InSb detector accessed ~2000 to 8000 cm^{-1}. A quartz lamp and quartz beamsplitter provided ~4000–13 000 cm^{-1}. A Si-avalanche detector was used for ~9000 to 22 000 cm^{-1}. Segments were merged and absorption coefficients (A) were calculated from thickness (L) using:

$$AL = -\log(I_{trans}/I_0). \quad (2)$$

Laser-flash analysis and data processing

Thermal diffusivity was measured with an LFA 427 manufactured by Netzsch Gerätebau, Germany. Specimens are suspended in a graphite holder that allows analysis of a circular area with diameter of 6 or 10 mm. The sample is located in the hot-spot zone of a furnace and the temperature dependence of D is obtained by varying furnace temperature. A single pulse from an Nd-GGG laser heats the sample from below and as heat diffuses from the bottom to the top of the sample, emissions are monitored by an InSb detector mounted above the sample. Data were acquired in an Ar gas atmosphere as time-temperature curves, ~10^2–10^4 ms (Fig. 1). Temperature was measured using calibrated W-Re thermocouples, one located adjacent to the sample. Graphite coatings on the sample (needed to block laser light and to enhance absorption of the pulse as well as sample emissions) buffer the oxygen fugacity at high temperatures to C-CO. Thermal diffusivity values are accurate to 2%, as verified against opaque and soft standard reference materials. Uncertainty in D arises largely from that of sample thickness. For details and calibration procedures, see Blumm and Lemarchand (2002), Hofmeister (2006) and Pertermann and Hofmeister (2006).

Data were obtained at 50–100 °C intervals with three acquisitions at each temperature. The algorithm of Mehling et al. (1998) was used to extract thermal diffusivity from the time-temperature curves (Fig. 1). This accounts for both radiative surface losses to the surroundings and supurious radiative transfer through the sample between the top and bottom graphite coats, and allows for absorbance being frequency dependent, although detailed values of optical properties are not needed. The measured shape of the laser pulse was corrected for (Blumm and Opfermann 2002). The amount of direct radiative transfer is small to negligible at all T for the black hercynites and magnetites and for T < ~1500 K for pale colored spinels (see examples in Fig. 1). Runs were terminated when radiative transfer became too strong for the model to reproduce the raw data, thereby ensuring the accuracy of our results: see discussion for details.

Sample descriptions and characteristics

Major elements

Chemical compositions of the samples (Table 1) were determined by combining spectroscopic with electron microprobe analysis. For the five spinels, spectroscopic data (below) indicate that all iron is ferrous, and that gahnite probably has 0.005 Fe^{3+} per formula unit (pfu). Consequently, the tetrahedral site is slightly overfilled, suggesting that at least ~0.005 pfu Mg is octhedrally coordinated. Divalent cations of the hercynites and magnetites were assumed to sum to 1.00, and the trivalent occupancies were assumed to sum to 2.00. The five spinels, gahnite, and two magnetites have compositions close to end-member. The hercynites have significant substitution of Fe^{2+} for Mg in the tetrahedral site and trace amounts of Zn and Mn, whereas the octahedral site has significant Fe^{3+} and trace Cr and Ti; but, some Mg could be octahedrally coordinated, causing overestimation of ferric iron contents.

Spectroscopic characterization of transition metal ions and hydroxyl

Absorptions of Fe ions in the hercynites and magnetites were too intense to quantify at sub-millimeter thicknesses, although a trough was observed near 2000 cm^{-1} for hercynite C1 (not shown), consistent with absorption patterns for aluminous spinels (Fig. 2). A narrow peak near 1500 cm^{-1} seen in all aluminous samples is due to overtones of Al-O stretching modes.

Hydroxyl absorptions were not detected. Our spectrometer does not reach frequencies associated with d-d electronic transitions of Fe^{3+}. The rest of this section discusses d-d transitions of Fe^{2+} and Cr^{3+} and intervalence charge transfer in near end-member spinels and gahnite.

The red and pink samples have a singlet near 18 500 cm^{-1} and a rise toward the visible that is attributed to d-d transitions

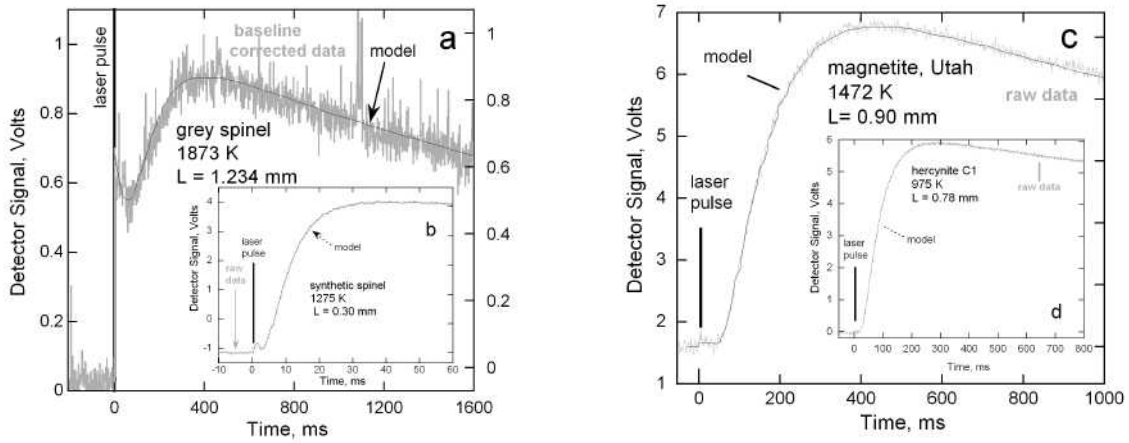

Figure 1. Temperature-time curves. Gray = raw data (except that a linear baseline was subtracted for gray spinel. Fine black or dotted line = model. Thick vertical line = laser pulse. Left panel = transparent spinels. Right panel = black spinels. (**a**) Gray spinel at one of the highest temperatures reached, with a large amount of radiative transfer (double arrow marked "c"). After reaching maximum temperature, emissions decrease as the sample re-equilibrates. (**b**) Synthetic spinel at moderate T, with a tiny amount of radiative transfer. The slower phonon travel occurs afterward, indicated by the dotted double arrow marked "u." Because this sample is very thin, rise times are fast. (**c**) Magnetite at high T with scant radiative transfer. (**d**) Hercynite at low T with negligible radiative transfer.

TABLE 1. Sample characteristics and electron microprobe analyses

Name	Location or origin	Composition (4 O basis)							Source	Description, lateral size
		Mg	Fe^{2+}	Zn	Al	Cr	Fe^{3+}	Ti		
Synthetic spinel	Union Carbide	1.0	–	–	2.0	–	–	–	R. Peterson	Colorless square, 7 mm
Pink spinel	Sri Lanka	1.004	0.004	0.002	1.99	0.004	–	tr	Ebay	Pink diamond, 6.5 mm
Red spinel	Sri Lanka	1.00	–	tr	1.95	0.034	0.01	tr	Ebay	Red, cracked triangle, 6 mm
Gray spinel	Unknown	0.96	0.01	0.02	2.01	tr	–	0.004	Burmagem	Silver oval, 9.5 × 11 mm^2
Blue spinel	Sri Lanka	0.98	0.03	tr	1.99	tr	–	tr	Bernie's Gems	Blue triangle, 7 mm
Gahnite	Brazil	0.009	0.04‡	0.957	1.99	–	0.01‡	–	NMNH 145883	Green heart, 6 mm
Hercynite C1	Parker Mine, Notre Dame du Laus, Quebec, Canada	0.804	0.174	0.022	1.890	0.001	0.102	tr	Tysons*	Black octagon, 7 mm
Hercynite T	That Nam Pehn, Thailand	0.765	0.221	0.013	1.836	0.002	0.151	0.011	Excaliber	Black irregular, 10 × 6 mm^2
Hercynite M	Fort Dauphin, Madagascar	0.725	0.257	0.018	1.929	0.001	0.070	tr	Wards	Black irregular, 6 × 9 mm^2
Hercynite U	Unknown	0.60†	0.395	0.002	1.726	–	0.247	0.027	U.C. Berkeley 3233	Black pentagon, 11 mm
Magnetite NY	Essex Co., New York	0.002	0.998	tr	0.008	tr	1.981	0.011	Washington U. 237-4	Black rectangle, 7 × 8 mm^2
Magnetite UT	Iron Mt., Utah	0.04	0.96	tr	0.01	tr	1.90	0.09	Excaliber	Black square, 8 mm

* A second crystal (hercynite C2) from the same locality was purchased from Wards, but not chemically analyzed. It melted at 1800 °C during data collection.
† Mn = 0.003.
‡ Spectroscopy suggests a slightly lower Fe^{3+} content of 0.005 pfu, which means that the Fe^{2+} content would be 0.045 pfu.

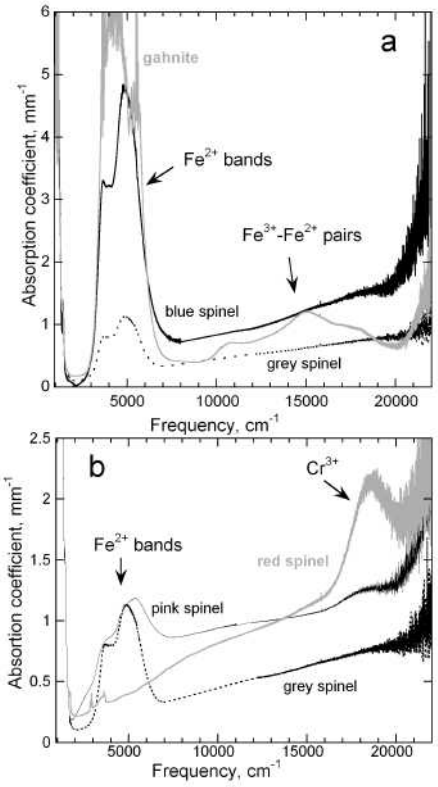

FIGURE 2. Absorption spectra scaled to represent thickness of 1 mm. (**a**) Samples lacking Cr^{3+}. Gahnite (gray line) data were collected from a sample with thickness of 0.74 mm, which is too thick to quantify the strong Fe^{2+} bands near 5000 cm^{-1}. Data for blue (solid black line) spinel was collected from a samples 0.4 mm thick. Data for gray spinel (dotted curve) was collected from samples between 0.576 and 0.883 mm thick. (**b**) Low Fe^{2+}-bearing samples. Dotted line = gray sample, described above. Gray curve = data collected from the red sample with thickness of 0.42 mm. Solid black curve = data collected from the pink sample with thickness of 1.075 mm.

of Cr^{3+} in the octahedral site. Microprobe analyses indicate that the red sample has 8.5 times more Cr than the pink sample, which is consistent with the ratio of the peak heights of 8.2:1 (red:pink) for the 18 500 cm^{-1} band (Fig. 2b). For the remaining spinels, Cr^{3+} was neither detected by electron microprobe nor spectroscopy.

The broad cluster of peaks with maxima occuring over 3600 to 5500 cm^{-1} is due to Fe^{2+} in the tetrahedral site (e.g., Skogby and Hålenius 2003; Taran et al. 2005). A singlet is expected and the existence of a multiplet was attributed to a dynamic Jahn-Teller effect by Slack et al. (1966), see discussion by Taran et al. (2005). The intensity of this cluster for the red sample, and therefore its Fe^{2+} content, is negligible. All Fe detected using microprobe analyses for the red sample (Table 1) is ferric. The intensity and Fe^{2+} content increases in the order: pink < gray < blue < gahnite, such that the pattern exhibited for the green gahnite sample differs slightly from the pattern found for paler spinels. However, this difference is probably an artifact of thickness because the gahnite transmission is nearly zero and a thicker blue sample (not shown) gave a pattern like that shown for gahnite (Fig. 2a) when its transmission was near zero. To estimate Fe^{2+} content in the tetrahedral sites of our samples, comparison is made with the most dilute spinel-hercynite solid solution of Hålenius et al. (2001): their sample with 0.02 Fe^{2+} pfu has A = 320/mm for the cluster peaking at 5200 cm^{-1}. The maximum absorbances of our lightly colored samples indicate contents in pfu Fe^{2+} of 0.0032 (pink), 0.0056 (gray), 0.028 (blue), and 0.036 for the gahnite. These values compare well with microprobe analysis of total pfu Fe of 0.004 (pink), 0.01 (gray), 0.03 (blue), and 0.04 (gahnite, Fe^{2+} only).

Gahnite has another band complex extending from ~11 000 to 18 000 cm^{-1} (Fig. 2). Similar patterns were observed for spinel-hercynite and gahnite-hercynite solid solutions with low total iron content (Taran et al. 2005). The spectrum for gahnite closely matches green type II samples of Taran et al. (2005), with bands at 10 890, 14 460, 18 380 cm^{-1} that were assigned to pairing of Fe^{2+} in the tetrahedral site with Fe^{3+} in the octrahedral site. This pattern was not seen for our pink, gray, and blue spinels, consistent with existence of Fe^{2+} only. For red spinel, this absence is consistent with existence of Fe^{3+} only. Our results differ from synthetics of $(Mg,Fe)Al_2O_4$ studied by Hålenius et al. (2001), which had higher Fe content and bands at 9500 and 14 000 cm^{-1} that they assigned to intervalence charge transfer between Fe^{2+} and Fe^{3+}, both in the octahedral site. The increase

in absorbance of our blue spinel and green gahnite toward the visible is compatible with absorptions of Fe^{3+} clusters observed for synthetic $Mg(Al,Fe^{3+})_2O_4$ (Andreozzi et al. 2001), but our instrument does not reach sufficiently high frequency to make a direct comparison. Therefore, Fe^{3+} is estimated through comparison with sample no. 7 of Taran et al. (2005) with 0.017 Fe^{3+} per 4 O atom formula unit and an absorption coefficient of 200/mm for the peak at 15 000 cm^{-1}. Our gahnite with A = 53/mm should have 0.005 Fe^{3+} pfu: the value of 0.01 from microprobe analysis is reasonably close, given the uncertainties in both approaches.

Literature values for Mg-Al disorder in spinel and hercynite

The amount of Mg-Al disorder in synthetic and natural aluminous spinels and its dependence on temperature has been primarily determined via X-ray diffractometry. Disorder is represented by the amount of Al in the tetrahedral site (x), which is refined by assuming that the scattering lengths of Mg, Al, and O are independent of T and of the site occupied by the cations (see Redfern et al. 1999). Disagreement exists among values of inversion parameters, and disordering rates differ among samples and studies, but roughly the same increase in x of ~0.16 pfu from 298 to ~1200 K is seen for all studies (Carbonin et al. 2002).

Synthetic, sintered, end-member hercynite initially has x ~0.12, which increases above ~900 K to 0.22 pfu at 1400 K (Harrison et al. 1998). Natural hercynite with large amounts of Fe^{2+} (0.22 pfu) but low Fe^{3+} (similar to hercynite C1 or T) initially has x = 0.12, which increases above 900 K to 0.24 pfu by ~1150 K (Della Guista et al. 1996). For synthetics across the spinel-hercynite join, x at 298 K decreases from 0.22 to 0.18 pfu as Fe increases (Andreozzi and Luccesi 2002). Natural spinel with Cr contents like our red spinel, but lacking Fe^{3+}, initially had x = 0.12, which increases above 900 K to ~0.28 pfu near ~1150 K (Carbonin et al. 2002). Martignago et al. (2003) studied three samples with varying Cr contents and found that all initially have x ~0.12, which increases above 970 K to ~0.29 at 1300 K. Their ferric sample (0.08 pfu) behaves similarly, but disorders at lower T of 825 K. Carbonin et al. (2002) found that synthetic, flux grown $MgAl_2O_4$ behaved similarly to their natural Cr spinel. From neutron diffractometry on Union Carbide $MgAl_2O_4$, initially x was 0.12 pfu, increasing to 0.20 at 900 K, and to 0.32 at 1300 K (Peterson et al. 1991). A single-crystal synthetic had x = 0.08 at 800 K, increasing to 0.25 at 1900 K (Yamanaka and Takéuchi 1986). Sintered polycrystals initially have x = 0.15 pfu, increasing to 0.35 pfu from 1000–1900 K (Redfern et al. 1999).

A few studies utilize nuclear magnetic resonances (NMR). Wood et al. (1986) found high x values for sintered $MgAl_2O_4$, but as discussed by Millard et al. (1992), these results are artificially elevated by use of large pulse widths. Millard et al. (1992) found that sintered spinel has x = 0.22 pfu at 700 K, increasing with T to a constant value of ~0.28 from 1000–1400 K. Natural near-end member spinel had x = 0.05 initially, which increases at T above ~800 K to ~0.35 pfu by ~1400 K, but did not change upon further heating to 1900 K (Maekawa et al. 1997). Minor element analysis detected 0.004 pfu Fe, which is probably divalent since the Mg^{2+} site was not filled. Its pale pink color requires a similarly small amount of Cr: this information combined with the presence of Fe^{2+} suggests a close comparison with our pink spinel.

Sintered synthetics, natural and synthetic single crystals appear to all have about the same amount of disorder at high temperature, regardless of differences in minor or major element chemistry. Some variation exists at low temperature, but an obvious correlation with chemistry is not evident in published literature. Clearly, all samples disorder significantly at temperatures between ~800 to 1000 K, the amount of disordering usually lessens above 1500 K, and thermal equilibrium is eventually obtained, but the disorder depends on the sample history. Probably, initial values depend on the thermal history of the sample prior to structural study.

Given the above and that our experiments are time dependent in a way that changes from run to run, it is not possible to quantify the amount of disorder accompanying the runs, unless we had split the sample and acquired NMR or crystallographic data at similar heating rates. Most of our samples were not large enough to split. For the hercynites, multiple site occupancies and charge states make quantifying disorder equivocal unless Fe^{3+} content is independently constrained (Harrison et al. 1999). Therefore, we isolated the effect of disorder on D from that of simply elevating temperature by (1) analyzing results at temperatures below those at which disordering is observed, and (2) analyzing our results obtained on samples that appeared to be fully (equilibrium) disordered, i.e., once a sufficient number of runs were made that D values no longer differed during the heating and cooling portions of the final experimental run.

THERMAL DIFFUSIVITY RESULTS

Thermal diffusivity is highest at room temperature, and decreases with rising temperature, such that the slope $\partial D/\partial T$ generally decreases as T increases (Figs. 3–5). Above ~1500 K, thermal diffusivity became constant (D_{sat}) within the uncertainties of measurement for the gray spinel which was equilibrium disordered during multiple heating runs. Saturation occurs above 1800 K for C2 hercynite, and 1000 K for magnetite. For the other samples, a weak dependence of D is seen at high temperature, but saturation was not reached. A lambda curve, due to the ferrimagnetic transition, is superimposed on the curve for $1/D$ vs. T for magnetite, see below. Table 2 provides information on the experimental runs, room-temperature values (D_{298}), D_{sat}, and curve fits. Most results are best represented by a linear fit of $1/D$ to a low-order polynomial in T, as observed for garnets (Hofmeister 2006). For samples that reached saturation, the fit describes the curvature below saturation, as indicated in Table 2.

Near end-member aluminous samples

Both minor element substititution and Mg-Al disorder affect thermal diffusivity. The large number of spinels near $MgAl_2O_4$ and $ZnAl_2O_4$ allow these effects to be distinguished.

At 298 K, D decreases in the order pink > gray > red > gahnite > synthetic > blue, which mostly correlates with the impurity content of 0.01 > 0.034 > 0.044 > 0.059 > 0 > 0.04 pfu. The synthetic is disordered as shown by neutron powder diffraction of the same material (Peterson et al. 1991). The gray and pink samples disordered significantly upon heating, which suggests that the initial amount of Al on Mg site is low. For gahnite, D_{298} changed only slightly upon heating (Fig. 3 inset), which suggests that it was only somewhat disordered during heating, even

TABLE 2. Run conditions and fits to thermal diffusivity at temperature

Name	Run No.	L mm	D_{298} mm²/s	D_{sat} mm²/s	T_{sat} K	Fit of 1/D vs. T s/mm²	$T_{fit,max}$ K	Notes
Synthetic	1	0.30	5.279	–	–	$-0.028815 + 0.00080365T - 9.7093 \times 10^{-8}T^2$	1394	Both runs on same trend
	2	0.285						
Pink	1	1.075	7.615	–	–	$-0.061134 + 0.00064676T$†	700	Drop in D at 1000 K
	2	1.075	5.354			virtually the same as synthetic	1161	High T and 2nd run coincide
Red*	1	0.668	6.04	–	–	$-0.08405 + 0.00084979T$	493	D uncertain due to fractures
	2	0.640	6.34			–		2nd run room temperature only
Gray	1	1.86	7.143	1.07	1550	$-0.19031 + 0.0013219T - 6.4564 \times 10^{-7}T^2$	520	Fit to T below disordering.
	8	1.234	5.12			$-0.10063 + 0.0010566T - 2.7092 \times 10^{-7}T^2$‖	1850	Last run and previous run >500 K
Blue	1	0.55	4.79			$-0.018854 + 0.00084926T - 1.6693 \times 10^{-7}T^2$	1069	Both runs follow same trend
	2	0.405	4.80			–		
Gahnite*	1	0.725	5.94			$-0.022985 + 0.00062933T$	670	Fit to T below disordering
	2	0.727	5.50			$-0.023369 + 0.00068785T$	1273	Cooling, similar to synthetic
Herc. C1		0.78	2.00	0.70‡	1750‡	$0.2942 + 0.00069598T$	800	D_{298} unchanged by heating
		0.78§	2.05§			$0.29973 + 0.00068264T$	1450	
Herc. T	1	0.735	1.75			$0.040141 + 0.0005734T$	550	Fit imperfect near 298 K
		0.68§	1.96§			$0.42934 + 0.00050009T$	1250	Fit imperfect near 1100 K
Herc. M	1	0.73	1.63			$0.3848 + 0.00076667T$	1000	Fit below 800 K
		0.73§	1.51§			$0.6935 + 0.00047878T$	1500	Fit above 1000 K
Herc. U	1	0.73	1.28			$0.30224 + 0.0020984T - 1.5109 \times 10^{-6}T^2$	550	Fit below 550 K
		0.73§	1.37§			#	1450	#
Magn. NY	1	1.05	2.04	0.730	1200	$-0.56653 + 0.0046202T - 3.4391 \times 10^{-6}T^2$**	500	Curie transition limits fit interval
	3	1.135	2.09					
Magn. UT	1	0.90	1.46	0.704	1000	$-0.033057 + 0.003049T - 1.8948 \times 10^{-6}T^2$	500	Curie transition limits fit interval
		0.88	1.41					

Notes: All fits had residuals better than 0.99.
* Small sample, results less accurate than ±2%.
† This trend best represents orderd spinel. It can also be fit to $D = 10460/T^{1.2721}$ or $D = 1/(0.00037364T + 2.8263 \times 10^{-7}T^2)$, shown in Figure 9b.
‡ Very high T data from sample C2, which melted. This sample seems to have the same composition than sample C1 from the same locality because both have the same D_{298} prior to heating. Sample C2 was heated to higher temperature in several runs and its trend for $D(T)$ differs from that of C1, see text.
§ For the hercynites, D was re-measured at 298 K only. For sample C1, no change in D_{298} was observed.
# Hercynite U has a non-linear trend even for the interval of 290–400 K. Over all temperatures measured (up to 1450 K), 1/D (in s/mm²) = $0.38549 + 0.0017926T - 1.5383 \times 10^{-6}T^2 + 5.598 \times 10^{-10}T^3$.
‖ This trend best represents (equilibrium) disordered spinel.
** Below 500 K, magnetite can be fit to $D = 1243.8/T^{1.1334}$ (gray line in Fig. 7).

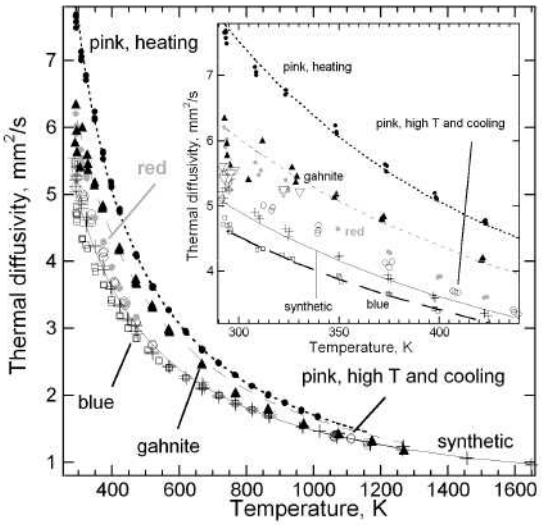

FIGURE 3. Thermal diffusivity of near end-member spinels (except for the gray sample) and gahnite as a function of temperature. Symbols indicate individual data points. Dotted line = curve fits of Table 2 for pink spinel. Solid line = curve fit for disordered synthetic spinel. Filled circles = pink spinel before disordering. Open circles = pink spinel after disording at high T. Gray circles = red spinel, low-T run. Open squares = blue spinel, both heating runs. Plus signs = synthetic spinel, both heating runs. Triangles = gahnite, first heating run. Inset = expanded view of low-temperature data showing the curve fit for the blue sample (dashed line). Open triangles = cooling run for gahnite. Above ~1000 K, all samples follow the same trend. Samples with lower amounts of impurities have higher D at 298 K.

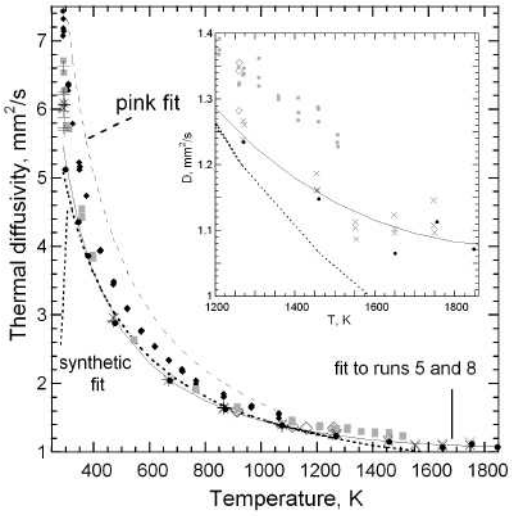

FIGURE 4. Thermal diffusivity of gray spinel showing the effect of progressive disordering during repeated heating. Filled diamonds = heating run 1 at low T. Open diamonds = high-temperature portion of run 1 and cool down. Gray squares = run 2. Plus signs = runs 3 (low temperature) and 4. X = run 5. (Run 6 is not shown because the thickness was incorrectly recorded.) Run 7 was acquired at room temperature only and is not shown for clarity. Filled circles = run 8, which show the average of each cluster of three data points at each temperature. All other symbols show individual measurements. Dashed line = curve fit for pink spinel. Dotted line = curve fit for synthetic spinel. Solid line = curve fit to runs 5 and 8 for the gray sample. Values of D did not change after 4 runs were made above ~1000 K.

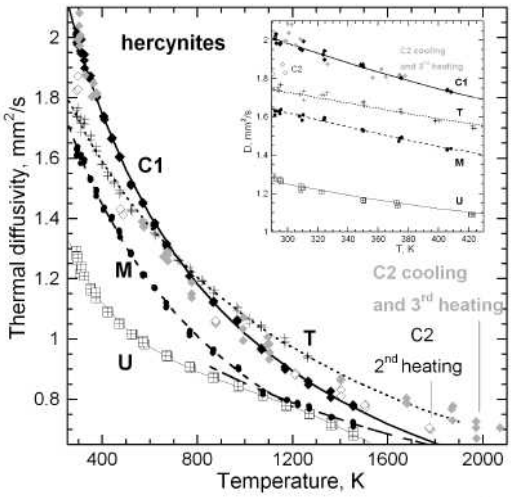

FIGURE 5. Thermal diffusivity of solid-solution hercynites. Filled diamonds = C1. Open diamonds = initial heating run of sample C2. Gray diamonds = data acquired upon cooling and reheating. The sample melted at the highest temperature of 2040 K. Plus sign = sample T. Filled circles = sample M. Squares = sample U. All symbols are individual data points. Curve fits (Table 2) are to 1/*D* over all temperature. Inset = expanded view at low temperature.

though it reached higher temperature than the pink spinel. This behavior is consistent with its low Mg content, because disorder decreases with substitution of Fe^{2+} for Mg (Andreozzi and Luccesi 2002), and Zn^{2+} should behave equivalently to Fe^{2+}, given its size. We suggest that gahnite is initially highly ordered. The red sample was not heated sufficiently to cause disorder, so it is unclear whether this sample is initially ordered or not, although structural studies of spinel with similar amounts of Cr indicate these have similar disorder as that of our synthetic (cf. Carbonin et al. 2002; Peterson et al. 1991). For the synthetic and blue spinels, high-temperature runs did not alter D_{298}, suggesting that these samples were initially disordered. From this information, the pink sample is the closest representation of highly ordered, near-end member spinel, consistent with structural studies of similar material (Maekawa et al. 1997). The decrease in D_{298} from the ordered pink to the gray samples of 0.47 mm^2/s nearly equals difference observed between the disordered synthetic and blue samples of 0.48 mm^2/s, and is attributed to the gray sample having 0.034 pfu more impurity atoms than the pink, and the blue having 0.040 pfu more impurity atoms than the synthetic. This behavior is consistent with the significant (~20%) change in D_{298} between pure forsterite and that doped with 0.3 wt% Co (Pertermann and Hofmeister 2006).

Above ~1200 K, *D* values for Al-rich spinels become nearly the same (Fig. 3 and 4). Similar behavior was observed for garnets and olivines, and is connected with the importance of the oxygen sublattice in heat transport. For spinel, convergence is also connected with disordering approaching equilibrium values, as is evidence by the sequence of high temperature runs on the gray sample. The highest temperature single data point at 1600 K for the synthetic is within the uncertainty of the larger number of measurements for the gray sample (cf. Figs. 3 and 4). For the gray, eight runs were made, six of which were at high enough temperature to augment disorder. The last two heating runs gave identical *D* values above 500 K (Fig. 4) and show that *D* is independent of temperature above 1550 K once disordering nears equilibrium. The high-temperature fit for gray spinel lies very close to the curve for the synthetic and best represents $D(T)$ for $MgAl_2O_4$ with equilibrium disorder. This fit also represents $ZnAl_2O_4$ above ~900 K.

The abrupt decrease in *D* for pink spinel just above 1000 K suggests that the fit to the initial heating run below this temperature (Table 2) represents $D(T)$ for highly ordered $MgAl_2O_4$. Support for this contention is provided by the trend for the pink sample merging with the low-temperature trend for gahnite near 1000 K, which should have little Mg-Al disorder, and that both of these trends project to *D* values that are slightly higher than *D* for disordered spinels above 1200 K (Fig. 3). The high-*T* trend for gahnite, which became slightly disordered at high temperature (after cooling, D_{298} is lower than the initial value), follows that of the disordered spinels (pink and gray after heating; blue and synthetic at all temperatures).

Natural, solid-solution hercynites

At room temperature, *D* of the hercynites is significantly lower than that of the near end-member Al-rich spinels (cf. Figs. 3–5, Table 2). The four samples studied in detail are solid solutions of $MgAl_2O_4$-$FeAl_2O_4$-$MgFe_2O_4$, such that amount of ferric iron in pfu is ~60% of the ferrous iron for samples C1, M, and U. Sample T has much less Fe^{3+} than the others. As Fe^{2+} content increases in the order C1 > T > M > U, *D* decreases monotonically (Fig. 5, inset). For low amounts of impurities, the change in *D* is rapid (Fig. 6), but is difficult to quantify given the large compositional gap between our spinels and hercynites and uncertainties in the amount of Mg-Al disorder in the hercynites. Given the temperature response discussed below and previous structural studies discussed above, we assume that the hercynites are Mg-Al disordered and link these to the synthetic and blue spinels. We cannot differentiate whether the total impurity content or the Fe^{2+} content largely controls D_{298}, because the Fe^{3+} content depends largely on the Fe^{2+} content, and because impurity ions other than Fe occur in small amounts (Table 1). Therefore, Figure 6 and Table 3 show fits based on substitution on the T site only as well as on the average substitution in both sites. Trends for ordered spinels at low impurity content are also shown and listed in the caption of Figure 6. These parallel the initial slopes for the disordered spinels.

As Fe^{2+} content increases toward the hercynite end-member, *D* should again rise, as suggested by $ZnAl_2O_4$ having D_{298} similar to that of spinel, by Fe and Zn having similar masses. Due to the large compositional gap, we did not include gahnite in the fitting.

Heating sample C1 to 1450 K did not seem to increase disorder, as D_{298} was unchanged afterward. However, heating another sample from the same locality (C2) to 1670 K did alter *D*. The initial value for C2 of 2.02 mm^2/s equals that of C1. This first run is not shown because the sample was overly thick (3.5 mm) causing uneven heating and scatter in the three data points at each temperature. After thinning C2 to 0.95 mm, *D* was remeasured: slightly lower values of *D* than those of C1 were obtained during heating to 1775 K (open diamonds in Fig. 5; D_{298} = 1.85 mm^2/s).

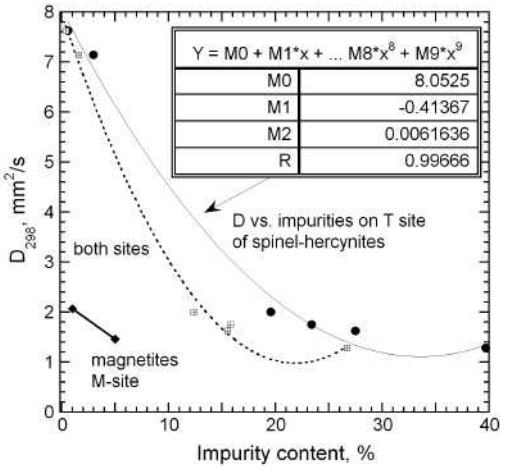

FIGURE 6. Thermal diffusivity of solid solutions as a function of impurity content. Diamonds = magnetites which only have detectable impurities (Ti) on their M sites. Other substitutions mostly involve Fe ions. Filled circles = disordered spinel-hercynites as a function of the impurity content, *x* as a percent on the T site. Squares with plus = disordered spinel-hercynites as a function of the average of the percent impurities on the T and M sites. Open circles = ordered spinels as a function of substitution on the T site only. Filled squares = ordered spinels as a function of the average of the substitutions on the T and M sites. For synthetic spinel, impurity content is calculated from the disorder measured by Peterson et al. (1991).

TABLE 3. Compositional trends for mainly Fe substitution

Type	Site	Limit (%)	Fits to *D* (in mm²/s)*
Magnetite	M	~10	$2.2163 - 0.15125z$
Ordered spinel	T	~8	$7.74 - 0.2x$
Ordered spinel	M and T	~8	$7.78 - 0.4y$
Spinel†	M and T	~15	$7.7922 - 0.43811y + 0.019057y^2$
Disordered hercynites	T	~30	$5.3461 - 0.22607x + 0.003131x^2$
Disordered hercynites	M and T	~45	$5.3025 - 0.35247y + 0.0075752y^2$

* *z* indicates the % impurities on the M site only, *x* indicates the % impurities on the T site only; *y* represents the average of the % impurities on each of the T and M sites.
† Disorder represented as impurities, i.e., synthetic spinel has 0.12 pfu Al on the T site (Peterson et al. 1991).

During cooling, the *D* values were higher than its original values, and closer to that of sample C1 (gray diamonds in Fig. 5; D_{298} = 2.06 mm²/s). During the fourth and final run, sample C1 melted at 1975 K. Because the melt reacted with the graphite holder, sample C2 was not analyzed chemically, but its composition should be similar to that of C1.

From Table 2, D_{298} of sample T was larger after heating to 1270 K. The surface of sample M was pitted after heating to 1470 K, and D_{298} is slightly lower than the initial value of 1.63 mm²/s. Sample U behaved similarly.

Changes in D_{298} upon heating (Table 2) seem connected with the amount of Fe^{3+}, and the maximum temperature of the run. For samples with high Fe^{3+} (T and U), D_{298} increases after heating and $|\partial D/\partial T|$ is larger at 1200 K than at 1100 K (Fig. 5), whereas for equilibrium disorder or continuous disordering $|\partial D/\partial T|$ decreases as *T* increases (Figs. 3 and 4). For samples with low Fe^{3+} (M and the first heating run of C2), D_{298} decreases after heating and $\partial D/\partial T$ becomes flat at high temperatures (>1000 K for M; >1600 K for C2). Sample C1 was not heated as high as C2 (Fig. 5) and did not seem to be altered. Repeated heatings of C2 increased D_{298}.

Two processes occur that affect *D* in opposite directions: (1) disordering of Mg (or Fe^{2+}) with Al decreases *D,* and (2) disordering of electrons (which "moves" Fe^{3+} to the T site, and Fe^{2+} to the M site) increases *D*. The onset of changes in *D* at 800 K, with effects being obvious by 1000 K is compatible with structural studies (summarized above). Due to the limitation of our spectrometer to Fe^{2+} bands, this hypothesis cannot be tested. Clearly, Fe content, oxidation state, and the presence of two substitutions (Mg-Fe^{2+} and Al-Fe^{3+}) affect the behavior of the hercynites. Understanding these complexities requires examining a wider range of compositions and probably samples closer to either the spinel-hercynite or spinel-magnesioferrite binaries.

We suggest that the samples initially have some degree of Mg-Al disorder, because temperatures that reduce *D* are much lower than those affecting the spinels, expecially for sample C. Although uncertainties exist in quantifiying disorder through crystallographic studies of samples with mixed valence, our conclusion is compatible these previous efforts (Della Guista et al. 1996; Harrison et al. 1998; Andreozzi and Luccesi 2002). Curve fits derived from low temperature only (Table 2) should depict changes in *D* in the absence of possible disordering processes. Representations over all temperature are also given, and are shown in Figure 5.

Magnetite and its Curie transition

For near end-member magnetite from New York, *D* at 298 K is 25% larger than that of the Utah sample, which has 4–5% substitution on each site (Fig. 6, Table 2). The high-temperature values are closer (Fig. 7). Thermal diffusivity of magnetite depends on composition in the same manner, as did the hercynites and spinels (Fig. 6).

The function 1/*D* has the shape of a lambda curve with a maximum at 790 K, connected with the ferrrimagnetic transition in magnetite. For pure metals (Fe, Ni, Co), the decrease in 1/*D* at high temperature is nearly vertical, whereas in magnetite a gentle slope is seen. The magnetic transition is at 853 K, whereas the change in thermal diffusivity begins at 790 K. Different rates of disordering of the electrons with temperature are possibly connected with the difference. Coordinated study of magnetic properties, C_P, and *D* are needed to understand the microscopic processes, but such is beyond the scope of this report.

DISCUSSION

Isolation of vibrational from radiative transfer in LFA results and trends above 298 K

With the possible exception of gahnite, our samples are either (1) optically thin in the near-IR to visible region associated with blackbody emissions above 298 K, having moderately to weakly absorbing broad bands of transition metal ions (Fig. 2), and hence radiative transfer should be removed by Mehling et al.'s (1998) model, or (2) are effectively opaque (hercynites and magnetites) and thus the temperature-time curves depict vibrational transport only and are described by Cowen's (1963) model. Very tiny amounts of radiative transfer are apparent in the temperature-time curves for some of the hercynites near 1000 K, consistent with slight transparency in the near-IR, but not only

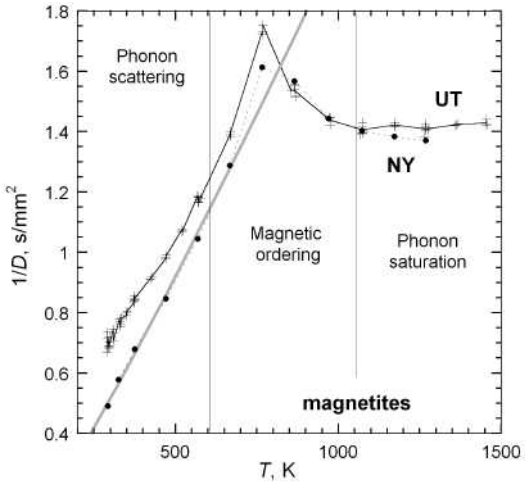

FIGURE 7. Inverse thermal diffusivity of magnetites as a function of temperature. Plus sign = individual data points for Utah magnetite. Filled circles = average of the 3–5 points collected at each temperature interval for the NY sample, with lower impurities. Black curves are spline fits. Gray line shows the fit to $D = 1243.8/T^{1.1334}$, which ignores low-T magnetic transitions. Vertical fine lines indicate the regions over which different processes control thermal diffusivity.

did the model of Mehling et al. (1998) fit the data well, but fits to Cowen's (1963) formulation departed only slightly from the data, and the difference in D obtained from these approaches is almost negligible. Nearly opaque solids can be represented by Mehling et al.'s (1998) model because their absorption spectrum very weakly depends on frequency. At very high T, temperature-time curves of the transparent samples are not fit well by Mehling et al.'s (1998) model. A less than perfect fit exists when the increase in emissions due to radiative transfer is over half of the total increase, and D so derived is less accurate than the 2% uncertainty associated with the technique. Data points involving excessive radiative transfer were not included in our analysis. Gahnite is optically thin at most frequencies, but has strong absorptions near 5000 cm^{-1} (Fig. 2) which may violate the optically thin conditions assumed by Mehling et al. (1998) and may cause model fits to imperfectly match the temperature-time curves. The sample diameter is small, which adds uncertainty due to edge effects being more important than in large samples. Given these two shortcomings in the gahnite data set, we estimated a larger uncertainty in D of 4% (Table 2). Observation of similar curves for $D(T)$ for both opaque, transparent, and partially transparent spinels with various cations and spectral characteristics (Figs. 3–5, and 7; Table 2) corroborates that radiative transfer is completely removed from the results for almost all cases (also see Blumm et al. 1997; Hofmann et al. 1998; Hofmeister 2006; Pertermann and Hofmeister 2006).

Such is not true for conventional methods involving contact, as suggested by previous observation of strong increases in $\partial D/\partial T$ with T at high T (e.g., Kanamori et al. 1968). Strong, positive slopes for $\partial D/\partial T$ at high T are not due to diffusive radiative transfer because some light crosses the small (~5 mm) samples in the laboratory unattenuated (as shown in Fig. 2 at ~2500 and ~8000 cm^{-1}; also see discussion of Pertermann and Hofmeister 2006), in violation of the requisite optically thick conditions (Hofmeister 2005). Consequently, previous contact measurements of D from single crystals above 298 K consist of unknown proportions of lattice and direct radiative transport. Spinel from Burma has a lattice constant indicating near end-member composition (Kanamori et al. 1968), and D at the lowest temperature measured using the Ångström method is bracketed by our gray and pink samples (Fig. 8), and therefore consistent with our results. However, $\partial D/\partial T$ obtained by Kanamori et al. (1968) is much lower, consistent with radiative transfer at elevated temperature. Near-IR spectra of spinel is highly transparent (Fig. 2), and our temperature-time curves (e.g., Fig. 1) show that some radiative transfer occurs even at low temperatures, ~400 K, for transparent spinel. High-temperature measurements of ceramic synthetic spinel (Anderson unpublished, provided by Slack 1962) lack this problem and are in good agreement with LFA data on disordered spinel (Fig. 9a).

From laser-flash measurements of spinels, $D(T)$ curves are sub-parallel (Figs. 3–5 and 8) such that the range in D among the various samples decreases with T. Similar behavior was seen in laser-flash results for olivine-family minerals (Pertermann and Hofmeister 2006) and chemically diverse garnets (Hofmeister 2006) and attributed to a correlation of D_{298} with $\partial D/\partial T$ at 298 K and to the dominance of the oxygen sub-lattice in controlling thermal diffusivity. At very high temperatures (~1900 K for hercynite, ~1500 K for spinel; ~1000 K for magnetite), $\partial D/\partial T$ approaches 0, as previously observed for garnets and olivines. The sub-parallel trends and asymptotic behavior are clearly intrinsic, given the diverse types of absorption spectra and intensity of absorptions present in the chemically distinct samples examined in diverse structures (22 garnets, 12 olivine group samples, and 12 spinels).

Comparison with previous single-crystal data for spinel and magnetite at 298 K and below

Finite losses of heat occur in measurements utilizing physical contact, as discerned from repeat measurements using multiple methods on nearly identical compositions (e.g., Lee and Hasselman 1985). Compared to LFA (Pertermann and Hofmeister 2006), D_{298} averaged for the three orientations of olivine (the most commonly studied mineral) is 7% lower when a single contact method is used (Gibert et al. 2005), but 22% lower if conventional, dual contact methods are used (average of D_{298} from Kanamori et al. 1968; Kobayashi 1974; Katsura 1995). Discrepancies for quartz and NaCl are similar, but lower (Hofmeister 2007). Comparison of all available single-crystal data suggests that spurious radiative transfer and contact losses both occur in contact measurements at 298 K, but in unknown proportions (Hofmeister et al. 2007). Cryogenic contact measurements of k_{lat} for garnets (Slack and Oliver 1971) and MgO (Slack 1962) agree reasonably well with laser-flash measurements, possibly because strong adhesives are used. We therefore make a detailed comparison to the results of Slack (1962), using Equation 1.

Heat capacity data of King (1954) from 53 to 296 K were joined by interpolation to C_P obtained from enthalpy measurements of Bonnickson (1954) from 421 to 1805 K, and the T^3 law was matched to the data near 60 K to provide a low T extrapolation. The results should be correct within a few percent except near 0 K. Thermal expansivity (α) from 320 to 1148 K

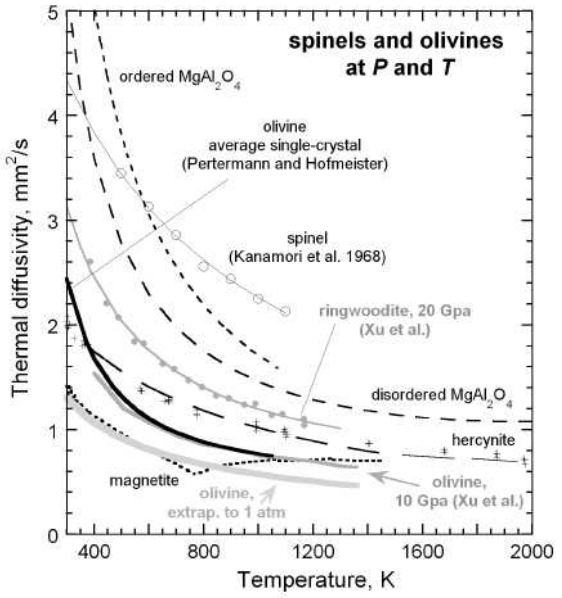

FIGURE 8. Comparison of laser-flash measurements of olivine and spinels to contact measurements at pressure. Broken lines are fits for the various types of spinels examined here. Dotted line = UT magnetite. Short dashes = natural pink spinel. Medium dashes = disordered synthetic and natural spinel. Long dashes and + signs = hercynite C1 and C2. Open circles = conventional measurements of spinel from Burma of Kanamori et al. (1968), which is fit to $1/D = 0.13935 + 0.00030321T$, shown as the very thin line. Thin gray line and dots = measurements of ringwoodite (Fo_{90} composition) at 20 GPa from Xu e al. (2005). Medium gray line = measurement of Fo_{90} olivine at 14 ceramic olivine at several high pressures to 1 atm. Heavy black solid line = average of the 3 orientations of laser-flash measurements on Fo_{90} at 1 atm from Pertermann and Hofmeister (2006).

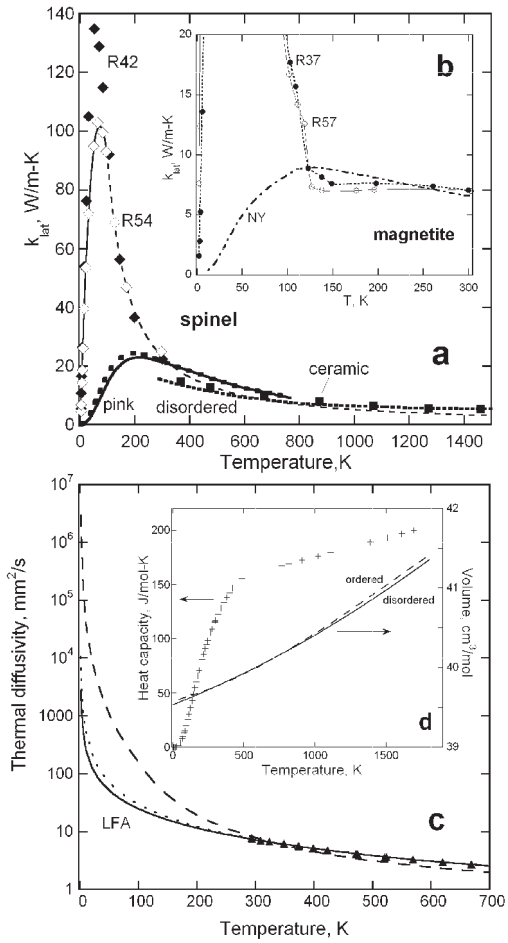

FIGURE 9. Comparison of cryogenic measurements with LFA data. (**a**) Thermal conductivity of spinel. Symbols are measured values of Slack (1962) obtained by digitizing. Diamonds = Burma gemstones. Fine solid line = $3.2096T - 0.028451T^2 + 2.5771 \times 10^{-5}T^3 + 3.8496 \times 10^{-7}T^4 - 9.0368 \times 10^{-10}T^5$. Fine dashed line = $27902T^{-1.2442}$. Squares = ceramic $MgAl_2O_4$ (Anderson 1952: not published, extracted from Slack 1962). Heavy solid line = calculated using a polynomial to LFA data on ordered pink spinel; heavy dots = power law: see footnotes of Table 2, and text. Long dashed line = calculated from fit to disordered spinel. (**b**) Thermal conductivity of magnetite. Circles = two samples from Slack (1962). Dot-dashed curve = fit of D from LFA to a power law (Table 2, Fig. 7), neglecting the Verwey transition at 120 K. (**c**) Thermal diffusivity of spinel on a logarithmic scale. Triangles = LFA data on pink spinel. Solid line = fit to polynomial with $1/D = 0$ at 0 K. Dotted line = power law fit. Dashed line = calculated from the fits in **a** to Burma spinel (Slack 1962). (d) Molar volume and C_P for spinel from literature data. See text for detailed description of sources and fits.

(Suzuki and Kumazawa 1980; Suzuki et al. 2000) were fit to a quadratic polynomial in T below 930 K and linearly above, to represent the ordered and disordered phases, respectively. For both cases, molar volume was obtained by integrating, using the definition, $\alpha = V^{-1}\partial V/\partial T$, and $V_{298} = 39.762$ cm^3/mol as the constant of integration. Volumes for the ordered and disorder phases differ negligibly and over 1800 K, V only changes from 39.6 to 41.5 cm^3/mol. Therefore, the uncertainty in calculating $\rho = M/V$ from extrapolating α is low, probably a few percent. For the ordered spinel, we extrapolate by fitting $1/D$ from 295 to 700 K to a power law and to a polynomial lacking a constant, so that $1/D \rightarrow 0$ as $T \rightarrow 0$ (fits are in the footnotes to Table 2). This limit assumes that phonon lifetimes change rapidly with temperature, and neglects scattering from crystal sides (see summary by Hofmeister 2006). At 298 K, our calculation is within the uncertainty of Slack's (1962) measurements of pink natural spinels from Burma, which are near end-member according to spectrographic analysis. Optical spectra of R54 (Slack et al. 1966) indicate a similar composition to our pink sample. Extrapolation to cryogenic values gives much lower k_{lat} with a maximum near 200 rather than 100 K (Fig. 9a). The two fits to our data on D give similar curves. The difference cannot be due to errors in C_P or V, which are small, so we also compare D extracted from Slack's results to our extrapolation (Fig. 9b). To make this comparison, we fit sample R54 to a fifth order polynomial (without a constant coefficient) at $T < 100$ K, and to a power law above 100 K, see Figure 9a. Except for the peak, the k_{lat} values are essentially the same for the two samples. The resulting thermal diffusivity (Fig. 9b) is 10^4 times larger than our extrapolation as $T \rightarrow 0$, ~10 times larger at 100 K, although at 298 K, D from Slack (1962) measurements matches ours. The extracted D of Slack is fit to $9.6105 \times 10^6 T^{-2.4353}$ in mm^2/s. From either comparison, the trends near 298 K in either D or k from

the cryogenic measurements change more rapidly with T than does the LFA data, suggesting that an additional, temperature dependent process affects Slack's (1962) measurements.

Possibly, contact resistance is T dependent and causes all discrepancies. However, it is highly likely that some degree of direct radiative transfer is present in the measurements of gemstones by Slack (1962). For spinel, direct radiative transfer occurs at 298 K in our experiments and at 400 K in those of Kanamori et al. (1968) (Fig. 8). Direct radiative transfer does not follow the T^3 law for diffusive transfer in a gray body (see Hofmeister 2005). We suggest that the match at 298 K with LFA data exists because contact resistance offsets the effect of radiative transfer.

Magnetite should not have radiative transfer because this mineral is opaque at the thicknesses used in all experiments. Comparison with contact methods is limited from 120 to 800 K, due to the Verwey transition and the Curie point occurring near these limits. Samples used in the various studies are all nearly end-member. To compute k_{lat}, we merged C_P above 298 K (Hemingway 1990) with cryogenic data from Westrum and Grønvold (1969). Fits to the unit-cell parameter from 120 to 800 K (Okudara et al. 1996) were used to calculate density (at 298 K, $\rho = 5.162$ g/cm^3 and $V = 44.528$ cm^3/mol). For the low-T extrapolation of our D data, the power law fit in Figure 7 was used. Reasonable agreement exists from 260–300 K (Fig. 9a, inset), given slight differences in sample compositions. Note that the Verwey transition affects Slack's (1962) data near 150 K, but our extrapolation neglects these phenomena. The better agreement for magnetite than spinel for temperatures of 120 to 300 K corroborates that radiative transfer likely affects Slack's (1962) data on spinel.

Comparison with the DHO-phonon gas model

The observed behavior is consistent with the damped harmonic oscillator model:

$$D(T) = \frac{< u(T) >^2}{6\pi Z < \mathrm{FWHM}(T) >} = \frac{< u(T) >^2 < \tau(T) >}{3Z} \quad (3)$$

where <u> is an average sound speed, Z is the number of formula units in the primitive cell, and <FWHM> is the average full-width at half maximum of the peaks in the dielectric function. Mean free lifetimes <τ> of the phonons decrease smoothly with T, largely due to increasing the number of states populated. Irrespective of the mismatch between cryogenic contact methods and LFA, the curves in D for spinels change smoothly and simply with T. The complicated dependence of k_{lat} on T results from combining the roughly inverse dependence of D on T with the "S" shaped curve of C_P and the very flat trend of V with T (Fig. 9b, inset). Given the simple response, one scattering mechanism occurs over all temperatures; the data show no evidence for distinguishing Umklapp and ordinary scattering events, at low and high T, respectively, as discussed in models based on acoustic modes (e.g., Burns 1990). Neither is there evidence of scattering from boundaries, as least above 3 K, from the comparison in Figure 9. The fits in Table 2 are consistent with this model, given that sound speeds change slowly with temperature and peak widths change rapidly (see discussion by Hofmeister 2006; Pertermann and Hofmeister 2006).

Thermal diffusivity approaches a constant above 1000 K for Fe-rich spinels and above 1600 K for the gray spinel, which was disordered during multiple heating runs. In the DHO model, this behavior is connected with saturation of the number of modes once the continuum becomes populated (Hofmeister 2006), and is analogous to the Dulong-Petit limit of heat capacity. As occurred for olivines (Pertermann and Hofmeister 2006) and garnets (Hofmeister 2006), the flat region occurs at roughly double the Debye temperature (which is ~660 K for Fe_3O_4: Kouvel 1956 and ~860 K for $MgAl_2O_4$: Anderson and Isaak 1995). The high-temperature asymptote was previously connected with the mean free path ($\lambda = u\tau$) approaching the size of the unit cell (or lattice constant) in the acoustic model (e.g., Ziman 1962). However, D_{sat} of magnetite and hercynite are nearly the same, although these have dissimilar lattice constants (8.39 and 8.10 Å, respectively, Okudara et al. 1996; Andreozzi and Lucchesi 2002), and spinel has D_{sat} larger by a factor of 2, although its lattice constant (8.08 Å) is close to that of hercynite. The DHO model is a better fit to the available data.

Thermal diffusivity of ringwoodite

Recently, D was obtained at P and T for olivine (Fo_{90}) and its high-pressure polymorphs (wadsleyite and the spinel form, ringwoodite) by Xu et al. (2004). Samples were fine-grained pressed ceramics and measurements were made at selected pressures over T from ~400 to 1150 K using the modified Ångström method, which involves two thermal contacts. Radiative transfer is not expected to be important, mainly because of the fine grain-size. The similar temperature derivatives for ringwoodite and the laser flash results on several spinel-type minerals corroborates that radiative transfer is low in the experiments of Xu et al. (2004). However, contact losses result in systematic underestimation of D for olivine by Xu et al. (2004). Specifically, D from their high-pressure measurements at 10 GPa match LFA data at 1 atm averaged for the three orientations (Fig. 8). This difference cannot be orientational, as their sample is a fine-grained ceramic. Moreover, measurements of each orientation of single-crystal olivine at 8.3 GPa by Osako et al. (2004), also using a contact method, nearly match the ambient pressure data. The single crystals have a very small amount of radiative transfer, which offsets some contact loss (seemingly 2 GPa worth).

Data on ringwoodite were gathered at 20 GPa and no other pressure by Xu et al. (2004). The formula of Hofmeister (1999)

$$\frac{\partial\left(\ln(k_{lat})\right)}{\partial P} = \frac{1}{K_T}\left(4\gamma_{th} + \frac{1}{3}\right) \quad (4)$$

and the approximate relationship $D^{-1}\partial D/\partial P = k^{-1}\partial k/\partial P - 1/K_T$ can be used to extrapolate these measurements to 1 atm. For hard solids, Hofmeister (2007) suggested a simple alternative:

$$\frac{\partial\left(\ln(k_{lat})\right)}{\partial P} \cong \frac{1}{K_T}\frac{\partial K_T}{\partial P} = \frac{K'}{K_T}. \quad (5)$$

This approximation omits terms ~1/10th of K'/K_T. Other formulas exist and are based on acoustic models. For example, Anderson (1989) provided

$$\frac{\partial\left(\ln(k_{lat})\right)}{\partial P} \cong \frac{1}{K_T}\frac{\partial K_T}{\partial P} + 2\frac{q_{th}}{K_T} + \frac{1}{K_T}\left(\gamma_{th} - \frac{4}{3}\right) \quad (6)$$

where the second Gruneisen parameter $q_{th} = -K_T\,\partial[\ln(\gamma_{th})]/\partial P$ is uncertain, varying from 0 to 4, depending on how it is determined

(see Hofmeister and Mao 2002). Acoustic models do not describe the existing data on solids at pressure as well as Equation 4 or 5, in part due to uncertainties in q_{th}, but several of these formula are dominated by the term K'/K_T.

The bulk modulus of ringwoodite is 184 GPa and K' is very near 4 (Sinogeiken et al. 2001; also see Hofmeister and Mao 2002) and the thermal Grüneisen parameter is 1.25 (Chopelas et al. 1994), giving the change in D as ~2.3%/GPa from Equation 4 and 1.6%/GPa from Equation 5, and thus the ambient pressure values should be 1.38 to 1.58 times those at high pressure. The projected value at 1 atm is then 2.0 to 2.3 mm^2/s, which is close to D_{298} of hercynite and olivine (Fig. 8), and clearly too low. All other parameters being equal, Equation 3 points to the spinel polymorph having k or D double that of olivine with the same composition. Thus, the measurements of Xu et al. (2004) must be corrected for contact loss. If we assume that the loss at high temperature is ~0.2 mm^2/s, as occurred for their olivines, then 1 atm values projected for ringwoodite lie just above the hercynite curve in Figure 8. This estimate is uncertain and also seems too low, given that our hercynite has extensive solid solution, and solid solutions reduce D (e.g., Fig. 6).

We provide three estimates of D at ambient pressure for ringwoodite by utilizing the compositional dependence of D_{298} at 1 atm (Fig. 6), the dependence of D_{298} on mass for olivines with <10 mol% substitution of Fe for Mg (Pertermann and Hofmeister 2006), and Equation 3. (1) Ordered spinel and γ-Mg_2SiO_4 have nearly identical masses and should therefore have the same D_{298} = 8 mm^2/s. This value is based on a small amount of impurities (~1 mol% in the spinel) and the presence of some disorder in γ-Mg_2SiO_4 (see Hazen et al. 1993). From the trends in Figure 6, substitution of Fe for Mg and exchange of Al and Mg have similar effects at the 10% level of the impurities on spinel: using the "ordered" curve, T site only, ringwoodite with composition Fo_{90} should have D_{298} = 5.6 mm^2/s, which is more than twice that of olivine with D_{298} = 2.4 mm^2/s, and very close to the initial value of equilibrium disordered spinel. However, this approach may have underestimated mass effects. (2) From Table 2 in Perterman and Hofmeister (2006), olivine has D_{298} that is 63% lower than that of Fo_{99} (cobalt doped), suggesting that ringwoodite should have D_{298} = 5.0 mm^2/s. We use the Co-doped forsterite because our spinel has a similar amount of impurities. (3) Equation 3 allows use of sound speeds to estimate D_{298} of silicate spinels from that of chemically equivalent olivine, because <FWHM> of olivines and silicate spinels are similar (u and FWHM are tabulated by Hofmeister 2001). For pure γ-Mg_2SiO_4, we predict D_{298} = 12.8 mm^2/s, for γ-Mg_2SiO_4, with ~1% cation impurities, we predict D_{298} = 10.3 mm^2/s, and for γ-$Mg_{1.8}Fe_{0.2}SiO_4$, we predict D_{298} = 6.7 mm^2/s, using $\langle u \rangle = (u_p + 2u_s)/3$. The mismatch of results from Equation 3 with our prediction of 8.0 mm^2/s for the impure gamma phase from D_{298} of pink spinel could be due to systematic variation in FWHM between the polymorphs or u differing from the weighted average of the sound speeds for either or both structures, and suggests that Equation 3 overpredicts D_{298} of ringwoodite by 20%, i.e., a value of 5.4 mm^2/s is more likely. This comparison further suggests that pure, ordered γ-Mg_2SiO_4 should have D_{298} near 10.2 mm^2/s.

The above estimates suggest an initial value of 5.3 ± 0.3 mm^2/s for ringwoodite with Fe/(Mg + Fe) ~0.1. For the temperature dependence, the $D(T)$ fit for gray, disordered spinel should be multiplied by 5.3/5.12. For the pressure dependence, Equation 4 is recommended (Hofmeister 2007).

Heat transport in Earth's transition zone

Diffusive radiative transfer, which is described as an effective thermal conductivity (k_{rad}) is important inside the Earth (Dubuffet et al. 2002). Because blackbody emissions depend entirely on temperature, k_{rad} is strongly T dependent and weakly P dependent (Hofmeister 2005). The pressure dependence of k_{rad} determined at 298 K from spectral data (e.g., Keppler and Smyth 2005), does not constrain the pressure dependence of k_{rad} at high T because peak positions of the blackbody emissions and mineral absorbance spectra overlap at high T, but not at 298 K. Due to the close tie of mantle pressures with temperatures, and to the form of the equations governing convection and conduction, the specific dependence of k_{rad} on T is needed to understand heat transport inside the Earth (see Dubuffet et al. 2002; Hofmeister and Yuen 2007). Spectra of ringwoodite have not yet been obtained at temperature. Given the similarity of its visible spectra to that of olivine, $k_{rad}(T)$ calculated for the lower pressure polymorph is a reasonable substitute. Values for garnet have yet to be determined. The remainder of this section concerns the lattice component expected for mixtures of garnet and ringwoodite.

Temperatures in the transition zone should exceed 1800 K, as suggested by experimental constraints of Katsura and Ito (1986) on the α-β transition at 13 GPa (410 km). Values at saturation therefore pertain, which are 1.07 mm^2/s for ringwoodite (discussed above) and 0.655 mm^2/s for upper mantle garnets (Hofmeister 2006), which should be similar to that of majoritic garnets (Giesting et al. 2004). From the compilation of Hofmeister and Mao (2003), transition zone garnets should have γ_{th} = 1.5, K''=4, and K_T = 165 GPa. Using Equation 4, we extrapolate D of ringwoodite and garnet to transition zone pressures, and calculate k_{lat} using densities from PREM, the high temperature for C_P of 1.3 J/g-K, which closely represents dense silicates (cf. Anderson and Isaak 1995;

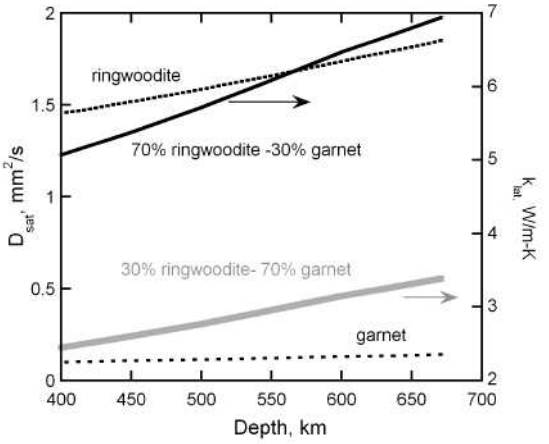

Figure 10. Lattice thermal conductivity in the transition zone. Calculations are based on Equations 1 and 4, and D_{sat} values obtained from analogues and response of D to disordering and cation substitution in Figure 6 and Equation 3. Broken lines = D of minerals. Solid lines = k_{lat} for end-member proportions suggested for the transition zone. See text for details.

Giesting et al. 2004), and possible proportions of these two major constituents. Given the approximate nature of this calculation, we neglect the stability of wadsleyite and the presence of pyroxene from ~410 to 510 km.

Figure 10 shows that the thermal conductivity in the transition zone depends on the proportion of ringwoodite. Because k_{rad} is roughly 1.2 W/m-K for the expected temperatures, grain-size and octahedral coordination of Fe^{2+} (Hofmeister 2005), the lattice component becomes increasingly important in governing heat flow and convection in the transition zone as the proportion of ringwoodite increases. Large amounts of ringwoodite are stabilizing against convection, especially as the darker, more Fe rich garnet phase should have lower k_{rad}. Our new measurements of *D* for spinel family minerals support the conclusions of Giesting et al. (2004), based on garnets, although the values for the transition zone are higher in the present paper, due to our new constraints on *D* of spinel family minerals.

Acknowledgments

I thank M. Pertermann and G. Benedix for obtaining electron microprobe analyses. This publication was supported by NSF grant EAR-0207198.

References cited

Anderson, D.L. (1989) Theory of the Earth, 366 p. Blackwell Scientific Publications, Oxford.

Anderson, O.L. and Isaak, D.G. (1995) Elastic constants of mantle minerals at high temperature. In T.J. Ahrens, Ed., Handbook of Physical Constants, p. 64–96. American Geophysical Union, Washington, D.C.

Andreozzi, G.B. and Luccesi, S. (2002) Intersite distribution of Fe^{2+} and Mg in the spinel (sensu stricto)-hercynite series by single-crystal X-ray diffraction. American Mineralogist, 87, 1113–1120.

Andreozzi, G.B., Hålenius, U., and Skogby H. (2001) Spectroscopic active $^{IV}Fe^{3+}$-$^{VI}Fe^{3+}$ clusters in spinel-magnesioferrite solid solutions crystals: A potential monitor for ordering in oxide spinels. Physics and Chemistry of Minerals, 28, 435–444.

Blumm, J. and Lemarchand, S. (2002) Influence of test conditions on the accuracy of laser flash measurements. High Temperatures–High Pressures, 34, 523–528.

Blumm, J. and Opfermann, J. (2002) Improvement of the mathematical modeling of flash measurements. High Temperatures–High Pressures, 34, 515–521.

Blumm, J., Henderson, J.B., Nilson, O., and Fricke, J. (1997) Laser flash measurement of the phononic thermal diffusivity of glasses in the presence of ballistic radiative transfer. High Temperature High Pressure, 29, 555–560.

Bonnickson, K.R. (1954) High temperature heat contents of aluminates of calcium and magnesium. Journal of Physical Chemistry, 59, 220–221.

Burns, G. (1990) Solid State Physics. Academic Press, San Diego

Carbonin, S., Martignago, F., Menegazzo, G., and Dal Negro, A. (2002) X-ray single-crystal study of spinels: In situ heating. Physics and Chemistry of Minerals, 29, 503–514.

Chopelas, A., Boehler, R., and Ko, R. (1994) Thermodynamics and behavior of γ-Mg_2SiO_4 at high pressure and implications for γ-Mg_2SiO_4 phase equilibria. Physics and Chemistry of Minerals, 21, 351–359.

Cowen, D.R. (1963) Pulse method of measuring thermal diffusivity at high temperatures. Journal of Applied Physics, 34, 926–927.

Della Giusta, A., Carbonin, S., and Ottonello, G. (1996) Temperature-dependent disorder in a natural Mg-Al-Fe^{2+}-Fe^{3+} spinel. Mineralogical Magazine, 60, 603–616.

Dubuffet, F., Yuen, D.A., and Rainey, E.S.G. (2002) Controlling thermal chaos in the mantle by positive feedback from radiative thermal conductivity. Nonlinear Processes in Geophysics, 9, 1–13.

Giesting, P.A., Hofmeister, A.M., Wopenka, B., Gwanmesia, G.D., and Jolliff, B.L. (2004) Thermal conductivity and thermodynamics of majoritic garnets: Implications for the transition zone. Earth and Planetary Science Letters, 218, 45–56.

Gibert, B., Schilling, F.R., Gratz, K., and Tommasi, A. (2005) Thermal diffusivity of olivine single crystals and a dunite at high temperature: Evidence for heat transfer by radiation in the upper mantle. Physics of the Earth and Planetary Interiors, 151, 129–141.

Hålenius, U., Skogby, H., and Andreozzi, G.B. (2001) Influence of cation distribution on the optical absorption spectra of Fe^{3+}-bearing spinel s.s.-hercynite crystals: Evidence for electron transitions in $^{VI}Fe^{2+}$-$^{VI}Fe^{3+}$ clusters. Physics and Chemistry of Minerals, 29, 319–330.

Harrison, R.J., Redfern, S.A.T., O'Neill, H.St.C., and Harrison, R.J. (1998) The temperature dependence of the cation distribution in synthetic hercynite ($FeAl_2O_4$) from in-situ neutron structure refinements. American Mineralogist, 83, 1092–1099.

Harrison, R.J., Dove, M.T., Knight, K.S., and Putnis, A. (1999) In-situ neutron diffraction study of non-convergent cation ordering in the $(Fe_3O_4)_{1-x}(MgAl_2O_4)_x$ spinel solid solution. American Mineralogist, 84, 555–563.

Hazen, R.M., Downs, R.T., Finger, L.W., and Ko, J. (1993) Crystal chemistry of ferromagnesian silicate spinels: evidence for Mg-Si disorder. American Mineralogist, 78, 1320–1323.

Hemingway, B. (1990) Thermodynamic properties for bunsenite, NiO, magnetite, Fe_3O_4, and hematite, Fe_2O_3, with comments on selected oxide buffer reactions. American Mineralogist, 75, 781–790.

Hofmann, R., Hahn, O., Raether, F., Mehling, H., and Fricke, J. (1998) Determination of thermal diffusivity in diathermic materials by the laser-flash technique. High Temperature High Pressure, 29, 703–710.

Hofmeister, A.M. (1999) Mantle values of thermal conductivity and the geotherm from phonon lifetimes. Science, 283, 1699–1706.

——— (2001) Thermal conductivity of spinels and olivines from vibrational spectroscopy at ambient conditions. American Mineralogist, 86, 1188–1208.

——— (2005) The dependence of radiative transfer on grain-size, temperature, and pressure: implications for mantle processes. Journal of Geodynamics, 40, 51–72.

——— (2006) Thermal diffusivity of garnets at high temperature. Physics and Chemistry of Minerals, 33, 45–62.

——— (2007) Pressure dependence of thermal diffusivity. Proceedings of the National Academy of Science, 104, no. 22 (DOI: 10.1073/pnas.0610734104).

Hofmeister, A.M. and Mao, H.K. (2001) Evaluation of shear moduli and other properties of silicate spinels from IR spectroscopy. American Mineralogist, 86, 622–639.

——— (2002) Redefinition of the mode Gruneisen parameter for polyatomic substances and thermodynamic implications. Proceedings of the National Academy of Science, 99, 559–564.

Hofmeister, A.M. and Yuen, D.A. (2007) Critical phenomena in thermal conductivity: Implications for lower mantle dynamics. Journal of Geodynamics, in press (DOI: 10.1016/j.jog.2007.03.002).

Hofmeister, A.M., Pertermann, M., and Branlund, J.M. (2007) Thermal conductivity of the Earth. In G.S. Schubert, Ed., Treatise in Geophysics, Chapter 48, in press.

Kanamori, H., Fujii, N., and Mizutani, H. (1968) Thermal diffusivity of rock-forming minerals. Journal of Geophysical Research, 73, 595–605.

Katsura, T. (1995) Thermal diffusivity of olivine under upper mantle conditions. Geophysical Journal International, 122, 63–69.

Katsura, T. and Ito, E. (1986) The system Mg_2SiO_4-Fe_2SiO_4 at high pressures and temperatures: Precise determination of stabilities of olivine, modified spinel, and spinel. Journal of Geophysical Research, 94, 15663–15670.

Keppler, H. and Smyth, J.R. (2005) Optical and near-infrared spectra of ringwoodite to 21.5 GPa: Implications for radiative heat transport in the mantle. American Mineralogist, 90, 1209–1212.

King, E.G. (1954) Heat capacities at low temperatures and entropies at 298.16 K of crystalline calcium and magnesium aluminates. Journal of Physical Chemistry, 59, 218–219.

Kobayashi, Y. (1974) Anisotropy of thermal diffusivity in olivine, pyroxene and dunite. Journal of Physics of the Earth, 22, 359–373.

Kouvel, J.S. (1956) Specific heat of a magnetite crystal at liquid helium temperatures. Physical Review, 102, 1489–1490.

Lee, H.L. and Hasselman, D.P.H. (1985) Comparison of data for thermal diffusivity obtained by laser-flash method using thermocouple and photodector. Journal of the American Ceramic Society, 68, C12–C13.

Maekawa, H., Kato, S., Kawamura, K., and Yokokawa, T. (1997) Cation mixing in natural $MgAl_2O_4$ spinel: a high-temperature ^{27}Al NMR study. American Mineralogist, 82, 1125–1132.

Martignago, F., Dal Negro, A., and Carbonin, S. (2003) How Cr^{3+} and Fe^{3+} affect Mg-Al order-disorder transformation at high temperature in natural spinels. Physics and Chemistry of Minerals, 30, 401–408.

Mehling, H., Hautzinger, G., Nilsson, O., Fricke, J., Hofmann, R., and Hahn, O. (1998) Thermal diffusivity of semitransparent materials determined by the laser-flash method applying a new mathematical model. International Journal of Thermophysics, 19, 941–949.

Millard, R.L., Peterson, R.C., and Hunter, B.K. (1992) Temperature dependence of cation disorder in $MgAl_2O_4$ spinel using ^{27}Al and ^{17}O magic-angle spinning NMR. American Mineralogist, 77, 44–52.

Okudara, H., Kihara, K., and Matsumoto, T. (1996) Temperature dependence of structure parameters in natural magnetite: single crystal X-ray studies from 126 to 773 K. Acta Crystallographica, B52, 450–457.

Osako, M., Ito, E., and Yoneda, A. (2004) Simultaneous measurements of thermal conductivity and thermal diffusivity for garnet and olivine under high pressure. Physics of the Earth and Planetary Interiors, 143–144, 311–20.

Parker, J.W., Jenkins, J.R., Butler, P.C., and Abbott, G.I. (1961) Flash method

of determining thermal diffusivity, heat capacity, and thermal conductivity. Journal of Applied Physics, 32, 1679–1684.
Pertermann, M. and Hofmeister, A.M. (2006) Thermal diffusivity of olivine-group minerals. American Mineralogist, 91, 1747–1760.
Peterson, R.C., Lager, G.A., and Hitterman, R.L. (1991) A time-of-flight neutron powder diffraction study of $MgAl_2O_4$ at temperatures up to 1273 K. American Mineralogist, 76, 1455–1458.
Redfern, S.A.T., Harrison, R.J., and O'Neill, H.St.C. (1999) Wood DRR Thermodynamics and kinetics of cation ordering in $MgAl_2O_4$ spinel up to 1600 °C from in situ neutron diffraction. American Mineralogist, 84, 299–310.
Sinogeikin, S.V., Bass, J.D., and Katsura, T. (2001) Single-crystal elasticity of γ-$(Mg_{0.91}Fe_{0.09})_2SiO_4$ to high pressures and temperatures. Geophysical Research Letters, 28, 4335–4338.
Skogby, H. and Hålenius, U. (2003) An FTIR study of tetrahedrally coordinated ferrous iron in the spinel-hercynite solid solution. American Mineralogist 88, 489–492.
Slack, G.A. (1962) Thermal conductivity of MgO, Al_2O_3, $MgAl_2O_4$, and Fe_3O_4 crystals from 3 to 300 K. Physical Review, 126, 427–441.
Slack, G.A. and Oliver, D.W. (1971) Thermal conductivity of garnets and phonon scattering by rare-earth ions. Physical Review, B4, 592–609.
Slack, G.A., Ham, F.S., and Chrenko, R.M. (1966) Optical absorption spectra of tetrahedral Fe^{2+} ($3d^6$) in cubic ZnS, CdTe, and $MgAl_2O_4$. Physical Review, 152, 376–402.
Suzuki, I. and Kumazawa, M. (1980) Anomalous thermal expansion in spinel $MgAl_2O_4$. Physics and Chemistry of Minerals, 5, 279–284.
Suzuki, I., Ohno, I., and Anderson, O.L. (2000) Harmonic and anharmonic properties of spinel $MgAl_2O_4$. American Mineralogist, 85, 304–311.
Taran, M.N., Koch-Müller, M., and Langer, K. (2005) Electronic absorption spectroscopy of natural (Fe^{2+}, Fe^{3+})-bearing spinels of spinel s.s.-hercynite and gahnite-hercynite solid solutions at different temperatures and high-pressures. Physics and Chemistry of Minerals, 32, 175–188.
Westrum, E.F. Jr. and Grønvold, F. (1969) Magnetite (Fe_3O_4) heat capacity and thermodynamic properties from 5 to 350 K, low-temperature transition. Journal of Chemical Thermodynamics, 1, 543–547.
Wood, B.J., Kirkpatrick, R.J., and Montez, B. (1986) Order-disorder phenomena in $MgAl_2O_4$ spinel. American Mineralogist, 71, 999–1006.
Xu, Y., Shankland, T.J., Linhardt, S., Rubie, D.C., Langenhorst, F., and Klasinski, K. (2004) Thermal diffusivity and conductivity of olivine, wadsleyite, and ringwoodite to 20 GPa and 1373 K. Physics of the Earth and Planetary Interiors, 143, 321–336.
Yamanaka, T. and Takéuchi, Y. (1983) Order-disorder in $MgAl_2O_4$ spinel at high temperatures up to 1700 °C. Zeitschrift für Kristallographie, 165, 65–78.
Ziman, J.M. (1962) Electrons and phonons: The theory of transport phenomena in solids. Clarendon Press, Oxford, U.K.

Manuscript received February 1, 2007
Manuscript accepted July 31, 2007
Manuscript handled by Guoyin Shen